

hep-lat/0412032
December 21, 2004

Center vortices and Dirac eigenmodes in SU(2) lattice gauge theory

**Jochen Gattnar^a, Christof Gattringer^b, Kurt Langfeld^a,
Hugo Reinhardt^a, Andreas Schäfer^b, Stefan Solbrig^b and T. Tok^a**

^a Institut für Theoretische Physik, Universität Tübingen
D-72076 Tübingen, Germany

^b Institut für Theoretische Physik, Universität Regensburg
D-93040 Regensburg, Germany

Abstract

We study the interplay between Dirac eigenmodes and center vortices in SU(2) lattice gauge theory. In particular we focus on vortex-removed configurations and compare them to an ensemble of configurations with random changes of the link variables. We show that removing the vortices destroys all zero modes and the near zero modes are no longer coupled to topological structures. The Dirac spectrum for vortex-removed configurations in many respects resembles a free spectrum thus leading to a vanishing chiral condensate. Configurations with random changes leave the topological features of the Dirac eigensystem intact. We finally show that smooth center vortex configurations give rise to zero modes and topological near zero modes.

PACS: 11.15.Ha

Key words: Lattice gauge theory, topology, center vortices, Dirac eigenmodes

1 Introduction and outline of results

The QCD vacuum has a highly non-trivial structure. Its excitations give rise to the key features of QCD, namely confinement and chiral symmetry breaking. Over the years, for both features several mechanisms have been proposed. For confinement the two most influential pictures are based on monopoles, respectively center vortices, while for chiral symmetry breaking instanton-type excitations have played a major role. It is widely expected that confinement and chiral symmetry breaking are linked through some unifying mechanism. This belief is supported by the fact that at the QCD phase transition deconfinement and restoration of chiral symmetry take place at the same critical temperature. However, our understanding of such a unifying mechanism is still in its infancy.

Lattice QCD is an important tool for analyzing excitations of the QCD vacuum and is even necessary for formulating some of the mechanisms such as the picture based on center vortices. Lattice simulations provide one with thermalized configurations of the gauge field as they appear in the path integral. These configurations can then be analyzed and one can try to identify the excitations of the gluon field relevant for different physical features.

Such lattice investigations have provided strong evidence for the center vortex picture of confinement. Vortices obtained after center projection in the maximum center gauge [1], are physical (in the sense of the renormalization group) [2], and seem to constitute the relevant infrared degrees of freedom of Yang-Mills theory. Indeed, when center vortices are removed from the Yang-Mills ensemble [3], the confinement properties are lost. The loss of confinement is indicated by the vanishing of the string tension and the change of the infrared behavior of the Green's functions in Landau gauge [4, 5] and in Coulomb gauge [6]. The emergence of a string tension can be easily understood in the center vortex picture. In addition, center vortices provide also an appealing picture of the finite temperature deconfinement phase transition as a depercolation transition in a 3-dimensional slice of the lattice universe, taken at a fixed spatial coordinate [7, 8]. Moreover, center vortices reproduce not only the correct order of the phase transition but also its universality class [9]. On the other hand in the spatial 3-volume, there is no depercolation transition and the center vortex ensemble correctly describes the increase of the spatial string tension above the critical temperature [10].

All these properties of center vortices detected on the lattice after center projection, as well as the correct order of the deconfinement phase transition are well reproduced in a random center vortex model for both $SU(2)$ [11] and $SU(3)$ [12]. Furthermore, the vortex percolation in the confinement phase is consistent with the vanishing of the free energy of center vortices in this phase as observed on the lattice [13] and in the continuum [14].

When center vortices are removed from the Yang-Mills ensemble, not only the string tension is gone but also the quark condensate vanishes and the topological charge is lost [3]. These findings suggest that center vortices could be responsible

for all infrared key features, confinement, chiral symmetry breaking and the chiral anomaly.

In $D = 4$ center vortices are closed flux surfaces, which act as wave guides for low-energetic quarks [15] and their percolation very likely triggers the condensation of quarks. Their topological charge can be understood in terms of their intersection number [17, 18] or, when center vortices are considered as time-dependent closed loops in 3-dimensional space, by their writhing number [18].

For the study of long range structures and topological excitations of the QCD vacuum, quantum fluctuations pose a serious challenge in the analysis of lattice configurations. These hard UV modes dominate the action and the long range structures are hidden under short distance noise. In recent years it has been understood that the low-lying eigenmodes of the lattice Dirac operator provide a natural filter sensitive to long range structures. These low-lying modes can be studied and information on the underlying IR structures of the gauge field can be extracted.

In this article we study the connection between center vortices and properties of Dirac eigenmodes for quenched $SU(2)$ configurations. In particular we apply the technique of Ref. [3] to remove the center vortices.

A central question of our article is how the removal of center vortices affects the long range topological structures of the Yang-Mills vacuum. As outlined, this question can be addressed through an analysis of the low-lying Dirac eigenmodes. We will show in this article that topological modes are destroyed when removing the center vortices. In particular the zero modes are gone completely. When analyzing the low-lying modes with non-vanishing eigenvalues, we find that their local chirality is gone and they do not resemble small perturbations of instanton-type zero modes.

For the spectrum of the Dirac operator we show that in many respects the spectrum of vortex-removed configurations resembles the spectrum of free fermions. This implies that the vortex-removed configurations cannot build up a non-vanishing chiral condensate via the Banks-Casher relation.

A legitimate criticism of removing the vortices is the fact that this procedure is a quite drastic modification of the gauge field. In this article we implement a crucial test by applying random changes to the original gauge configurations. In particular we multiply randomly chosen links of the lattice with the non-trivial center element. We demonstrate that to a large extent the topological information is stable under such random changes. The number of zero modes is essentially invariant and also the chiral properties of zero-modes and near zero-modes. Our test shows that the center vortices are correlated in a highly non-trivial way and their removal specifically destroys topological features of the gauge field configuration.

Finally we will demonstrate for smooth vortex configurations that they indeed give rise to zero modes of the Dirac operator. We analyze the procedures of center projection and vortex removal for these configurations. The findings for

the smooth configurations support our interpretation of the results for center projection and vortex removal applied to thermalized configurations.

Our article is organized as follows: In the next section we discuss technical aspects of our calculation, in particular the preparation of the original, the vortex-removed and the random-changed configurations, as well as the Dirac operator and the computation of the eigensystem. In Section 3 we discuss eigenvalue spectra and their interpretation. In Section 4 we present the observables based on the Dirac eigenvectors. In Section 5 we study Dirac spectrum and eigenmodes for the hand-constructed smooth vortex configurations. Our paper closes with a summary and the discussion of the results.

2 Technicalities

2.1 Preparation of the original ensembles

The SU(2) lattice configurations were generated with the standard heat bath algorithm using the Wilson action. After a careful thermalization, each “measurement” was taken after 20 dummy heat bath sweeps. We analyze a total of 100 quenched SU(2) configurations generated on a 12^4 lattice at $\beta = 2.5$.

2.2 Center vortices and their removal

The method of identification [1] and removal [3] of center vortices is based on the so-called maximal center gauge (MCG) [1, 16]. If

$$U_\mu^\Omega(x) = \Omega(x) U_\mu(x) \Omega^\dagger(x + \mu), \quad \Omega(x) \in \text{SU}(2) \quad (1)$$

denotes the gauge transformed link, MCG fixing is implemented by maximizing

$$S_{\text{fix}} = \sum_{x,\mu} \left[\text{tr} U_\mu^\Omega(x) \right]^2 \xrightarrow{\Omega} \max \quad (2)$$

with respect to $\Omega(x)$ thereby bringing each link as close as possible to a center element [16], or a given gauge field configuration as close as possible to a collection of center vortices [17]. This gauge condition was implemented by using an iteration-overrelaxation (IO) procedure (details are presented in [16]). The IO procedure was stopped when the difference between the variational action S_{fix} of two subsequent gauge fixing sweeps was smaller than 10^{-6} .

After MCG fixing the center vortices are identified by replacing each link $U_\mu^\Omega(x)$ by its closest center element $Z_\mu(x) \in Z(2)$, thereby each gauge configuration $U_\mu(x)$ is converted into an “ideal” center vortex configuration, consisting of closed hypersurfaces of plaquettes being equal to a non-trivial center element

$Z_\mu \neq 1$. The center vortex-removed theory [3] is defined by replacing the original gauge fixed links $U_\mu^\Omega(x)$ by

$$U_\mu^\Omega(x) \rightarrow Z_\mu^*(x)U_\mu^\Omega(x) , \quad (3)$$

where the $Z_\mu(x)$ are the center projected counter parts of the $U_\mu^\Omega(x)$. Let us emphasize that the vortex removal procedure [3] de facto removes the center projected image $Z_\mu(x)$ from the original gauge fixed configuration $U_\mu^\Omega(x)$.

2.3 Configurations with random changes

One has to keep in mind that removing the vortices is a drastic alteration of the gauge configuration: A large portion of the links is flipped, i.e. the links are multiplied by a factor of -1 . This change leads to a flip of about 3% of the plaquettes. The average plaquette drops by about 5 %, from 0.651 on the original configuration down to 0.621 after removing the vortices. It must be stressed, that the non-trivial center elements are highly correlated beyond the fact that the vortices form closed surfaces on the dual lattice. An important question is what the effects of a similar, but unstructured alteration of the lattice configuration will be.

To address this question we analyze the effect of uncorrelated random changes. The procedure for these random changes is somewhat similar to the prescription for removing the vortices. We first randomly choose a certain number N_{flip} of links (x, μ) where the random changes are implemented. For the selected links we change the corresponding link variables $U_\mu(x)$ according to

$$U_\mu(x) \rightarrow -U_\mu(x) , \quad (4)$$

i.e., we flip a randomly selected set of N_{flip} link variables. The number N_{flip} of randomly chosen links subject to the transformation (4) is a free parameter.

The number of flipped plaquettes increases quickly with the number N_{flip} of randomly flipped links. We find that randomly flipping $N_{flip} = 1000$ links on our 12^4 lattice (this is 1.2% of the total number of links) leads to a flip of about 4.6% of the plaquettes. This decreases the average plaquette by about 10%, from 0.651 on the original configuration to 0.590 after the random changes. Thus with our choice of $N_{flip} = 1000$ the random changes increase the action about twice as much as removing the vortices.

2.4 The eigensystem of the Dirac operator

For all four ensembles, original, center projected, vortex-removed and random-changed, we computed eigenvalues and eigenvectors of the chirally improved (CI) lattice Dirac operator [19, 20]. The CI operator is a systematic approximation of a solution of the Ginsparg-Wilson equation which governs chiral symmetry

on the lattice. The approximation is ultra-local and so allows for good chiral properties at a relatively low cost. The ultra-locality makes the CI operator also particularly suitable for the analysis of topological objects. In [21] it was e.g. shown that the CI operator provides a better lattice image of the continuum zero mode of instantons small in lattice units, when compared to the exactly chiral, but non-ultra-local overlap operator.

The actual calculation of the eigensystem was done with the implicitly restarted Arnoldi method [22]. For each configuration we calculated the 50 smallest eigenvalues and the corresponding eigenvectors. We vary the boundary conditions of the Dirac operator which is a powerful tool to probe the system [23]-[26]. While we keep periodic boundary conditions for the spatial directions, we allow for an arbitrary phase in the temporal direction. Thus the eigenvectors \vec{v} obey

$$\vec{v}(x + L\hat{i}) = \vec{v}(x), \quad i = 1, 2, 3 \quad ; \quad \vec{v}(x + L\hat{4}) = e^{i2\pi\varphi} \vec{v}(x), \quad (5)$$

where L is the size of our lattice and $\hat{i}, \hat{4}$ are the unit-vectors in the spatial, respectively the temporal directions. The phase factor φ can assume values between 0 and 1, and the special cases of $\varphi = 0$ and $\varphi = 1/2$ correspond to periodic, respectively anti-periodic temporal boundary conditions.

For a Dirac operator which obeys the Ginsparg-Wilson equation, the eigenvalues are restricted to the so-called Ginsparg-Wilson circle, a circle with radius 1 and center $(1, 0)$ in the complex plane. For the CI operator, which is an approximate Ginsparg-Wilson operator, the eigenvalues fluctuate around the Ginsparg-Wilson circle. In particular also the zero modes do not have eigenvalues that are exactly zero. In general they have a small, but non-vanishing real part. We stress, however, that there is no mixing of zero modes and near zero modes, since eigenvectors that correspond to eigenvalues with non-vanishing imaginary parts have an exactly vanishing matrix element with γ_5 and can be identified unambiguously. Thus eigenmodes with real eigenvalues are the would-be zero modes of the continuum.

3 Spectra of the Dirac operator

3.1 Spectra for center-projected configurations

As a first approach to analyzing the relation between center vortices and Dirac eigenmodes one can calculate the spectrum directly for the center projected configurations. The result of such a calculation is shown in Fig. 1, where in the right-hand side (rhs.) plot we superimpose spectra for 10 center projected configurations and compare them to the corresponding spectra of the original configurations (lhs. plot). All spectra were calculated using anti-periodic boundary conditions.

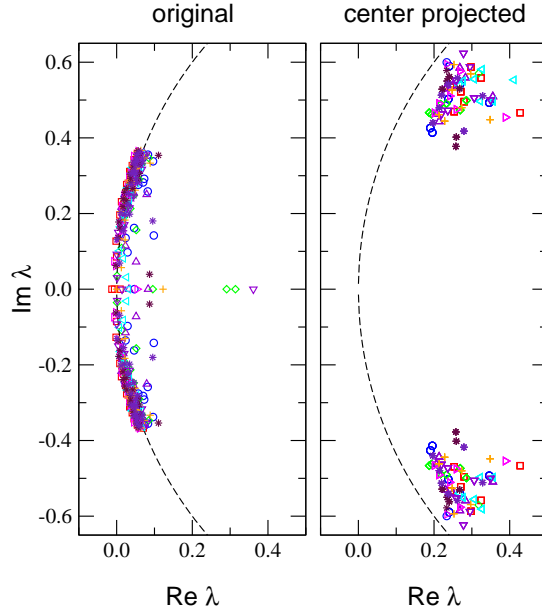


Figure 1: Dirac eigenvalues λ in the complex plane. We compare the spectrum for the original ensemble (lhs. plot) to the spectrum for center-projected configurations (rhs. plot). Each plot contains the 50 smallest eigenvalues for 10 different configurations with every configuration represented by a different symbol. Anti-periodic temporal boundary conditions were used for the Dirac operator.

In the lhs. plot for the original configurations one clearly sees that the eigenvalues cluster near the Ginsparg-Wilson circle (represented by the dashed curve) and only slightly scatter away from it (except for some real modes). The density of eigenvalues extends all the way to the origin indicating, that chiral symmetry is broken according to the Banks-Casher formula [27]. In addition we find several real eigenvalues, i.e. would-be zero modes corresponding to non-vanishing topological charge via the index theorem.

The spectra for the center projected configurations on the rhs. plot show a completely different picture. The spectra have developed a large gap, and all real eigenvalues are gone. The eigenvalues are concentrated in two clusters (symmetric with respect to reflection on the real axis). These clusters are shifted to large values of the imaginary parts, beyond the range for the eigenvalues for the original configurations. This hard to interpret outcome is not really a surprise: The Dirac operator, which contains the gradient operator, can detect only smooth topologically non-trivial structures. The center projected configurations are, however, maximally discontinuous. The link variables can only jump from $+1$ to -1 when going from a link to its neighbors. Obviously, the spectrum of the Dirac operator, which is to a high degree determined by topological properties of the gauge field, is sensitive to the discontinuity of the link variables. Thus we conclude that analyzing the Dirac spectrum directly for center projected configu-

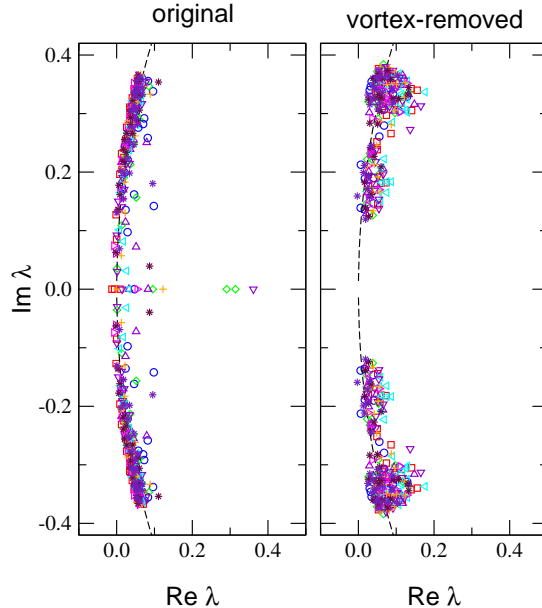


Figure 2: *Dirac eigenvalues λ in the complex plane. We compare the spectrum for the original ensemble (lhs. plot) to the spectrum for vortex-removed configurations (rhs. plot). Each plot contains the 50 smallest eigenvalues for 10 different configurations, with every configuration represented by a different symbol. Anti-periodic temporal boundary conditions were used for the Dirac operator.*

rations is a failed, although instructive attempt. We will come back to this issue in Section 5.

3.2 Spectra for vortex-removed configurations

A way to study the role of center vortices without the drastic measure of projecting the gauge links onto their center elements is the technique of removing the vortices outlined in Section 2.2. Although this procedure also introduces short range disorder, the changes are by far not as drastic as for center projection (at least as long as the vortices are not too fat, see below for more details), and one expects the approach via the analysis of Dirac eigenmodes to be viable.

In the rhs. plot of Fig. 2 we show superimposed the spectra for 10 vortex-removed configurations and in the lhs. plot the spectra for the corresponding original configurations. We use the same set of configurations already used in Fig. 1 (note that we have changed the vertical scale), and again apply anti-periodic temporal boundary conditions. Now the situation in the rhs. plot is quite different from the situation in the rhs. plot of Fig. 1. In particular the spectrum does not display the strong shift towards large imaginary parts, and essentially stays in the same range as the original spectra. Also the eigenvalues are still quite close to the Ginsparg-Wilson circle. However, again we observe a

gap in the spectrum, indicating that on the vortex-removed configurations the chiral condensate vanishes.

A crucial observation that can be made, is the fact that the eigenvalues fall into clusters. It is particularly interesting to count the number of eigenvalues in the lower cluster (and its mirror image obtained by reflection at the real axis). One finds that this occupation number typically is 8 eigenvalues per configuration for this lowest cluster.

In an attempt to understand this occupation number of the lowest cluster we now look at the spectrum for the free case, which can be calculated using Fourier transform. Since we are only interested in the lowest eigenvalues, we can ignore the effects of the periodicity of the Brillouin zone caused by the lattice and work with the continuum form $\widehat{D}(p) = ip_\mu \gamma_\mu \times \mathbf{1}_2$ of the Dirac operator in momentum space. The factor $\mathbf{1}_2$ is a 2×2 unit matrix coming from the trivial SU(2) field configuration. The eigenvalues of $\widehat{D}(p)$ are given by

$$\lambda = \pm i \sqrt{p_1^2 + p_2^2 + p_3^2 + p_4^2}. \quad (6)$$

Note that each eigenvalue is 4-fold degenerate, where a 2-fold degeneracy follows from the block-diagonal structure of the γ -matrices, and another 2-fold degeneracy from the trivial SU(2) color structure. For the momenta p_μ we insert the discrete momenta allowed on the lattice. These momenta are sensitive to the boundary conditions we use. In particular we find (compare Eq. (5) for the definition of the boundary condition parameter φ)

$$p_i = \frac{2\pi}{aN} k_i, \quad i = 1, 2, 3, \quad p_4 = \frac{2\pi}{aN} (k_4 + \varphi) \quad \text{with} \quad k_\mu = 0, \pm 1, \pm 2 \dots \quad (7)$$

Here N is the total number of lattice points in one direction and a denotes the lattice spacing, i.e. the physical extension L of our lattice is $L = aN$.

Let us now analyze what degeneracy of the smallest eigenvalue we find for the anti-periodic boundary conditions used in Fig. 2. For this case we have $\varphi = 1/2$. We find a 4-component of the momentum of $p_4 = \pi/aN$ for $k_4 = 0$ and $p_4 = -\pi/aN$ for $k_4 = -1$. These two values differ only by a sign, and since the eigenvalues (6) depend only on the square p_4^2 we find an extra degeneracy of the lowest eigenvalue (defined by $p_1 = p_2 = p_3 = 0, p_4 = \pm\pi/aN$). Thus for anti-periodic boundary conditions we obtain an 8-fold degeneracy as observed in the lowest clusters in the rhs. plot of Fig. 2.

It is tempting to interpret the eigenvalues in the rhs. plot of Fig. 2 as a slightly disturbed free spectrum. If indeed removing the vortices removes all topological excitations, then one would expect that the remaining configuration is essentially a trivial configuration plus some fluctuations. In order to test the hypothesis, that after removing the vortices one is essentially left with a free spectrum, we now use different values for the boundary condition parameter φ . For a value of $\varphi = 0$ (periodic boundary conditions) we again obtain an 8-fold degeneracy, since

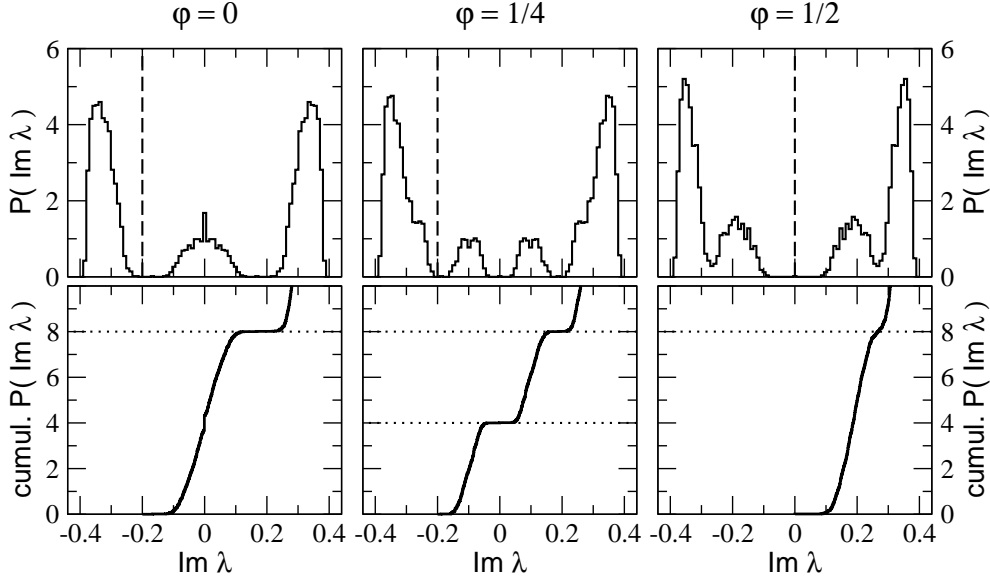


Figure 3: *Histograms (top row) and cumulated histograms (bottom row) of the imaginary parts of Dirac eigenvalues for vortex-removed configurations. We compare the histograms for periodic ($\varphi = 0$) b.c. (lhs. plots), for $\varphi = 1/4$ (center plots) and for anti-periodic ($\varphi = 1/2$) b.c. The vertical dashed lines in the top row plots show where we started with summing the numbers for the cumulative histograms. In the cumulative histograms (bottom row) we use dotted horizontal lines to indicate where the cumulative histogram exhibits a shoulder.*

for $p_1 = p_2 = p_3 = p_4 = 0$ the two signs in (6) both give $\lambda = 0$. For the case of $\varphi = 1/4$ we obtain only 4-fold degeneracy of the lowest eigenvalue characterized by $p_1 = p_2 = p_3 = 0, p_4 = \pi/(2aN)$.

To make our study more quantitative we present our results for the spectra now as histograms using all 100 configurations which we analyzed. In particular we use two types of histograms: Histograms where the density of the eigenvalues is plotted as a function of $\text{Im}\lambda$, and cumulative histograms where the total number of eigenvalues below a certain value of $\text{Im}\lambda$ is shown. For the vortex-removed configurations the results are shown in Fig. 3 with the regular histograms in the top row and the corresponding cumulative histograms in the bottom row. The three columns of plots are for the three different boundary conditions we used (from left to right: $\varphi = 0, \varphi = 1/4, \varphi = 1/2$).

The three regular histograms in the top row are symmetric with respect to reflection at the origin due to the corresponding symmetry of the spectrum. The histograms show a clear separation of several maxima, with the position of the maxima changing as a function of φ . The position of the lowest maxima is qualitatively at the same position as for the free case where $\lambda = 0$ for $\varphi = 0$, $\lambda = \pm i\pi/(2aN)$ for $\varphi = 1/4$ and $\lambda = \pm i\pi/aN$ for $\varphi = 1/2$. We remark that the

50 eigenvalues, available for each of our configurations, are not enough to obtain all eigenvalues in the cluster corresponding to the second-smallest free eigenvalue. For example in the case of $\varphi = 0$ the second-smallest eigenvalue, characterized by one of the p_μ being $2\pi/aN$, the others being equal to 0, is already 32-fold degenerate. Since this eigenvalue comes as a complex conjugate pair, we find a total of $8 + 2 \times 32 = 72$ eigenvalues in the two smallest eigenvalues (the larger one being a complex conjugate pair). Thus with our 50 eigenvalues the second cluster is not completely filled and the larger peaks in the top row of histograms in Fig. 3 correspond to only a subset of eigenvalues expected.

Let us now analyze the occupation numbers in the lowest cluster for the different boundary conditions. We start summing our cumulative histograms in the minimum below the clusters we are interested in. In the top row plots of Fig. 3 we mark this position by a vertical dashed line. The corresponding cumulative histograms are shown right below the regular histograms. For the case of $\varphi = 0$ we find that the cumulative histogram shows a pronounced shoulder at a value of 8 (the cumulative histogram was normalized by the total number of configurations). This shows clearly that the lowest cluster of eigenvalues has an occupation number of 8, matching the degeneracy of the lowest eigenvalue in the free case. For $\varphi = 1/4$ the histogram shows shoulders at 4 and 8, again matching the degeneracies of the free case. Finally for $\varphi = 1/2$ we do not see a clear shoulder but at least a pronounced dip in the curve. The reason is that for this case the lowest and the second eigenvalue are relatively close to each other and we do not have a clean separation of the two clusters, as can already be seen in the corresponding regular histogram.

To summarize, the relative position of the peaks in the regular histograms, as well as the occupation number in each cluster as obtained from the cumulative histograms, leads to the conclusion that the spectrum for vortex-removed configurations strongly resembles a free spectrum, slightly perturbed by fluctuations. This finding has two important physical implications: Firstly, we conclude that no topological objects are left in the gauge configurations after center vortices have been removed. The few zero modes (i.e., real modes on the lattice) that are found for $\varphi = 0$ (see Fig. 3) are the trivial zero modes present also for the free Dirac operator. For the other boundary conditions the complete absence of zero modes already shows the absence of topological charge via the index theorem. Secondly, the fact that the spectral density near the origin behaves like in the free case shows that the chiral condensate vanishes for vortex-removed configurations which strongly supports the findings of [3].

For completeness we show the histograms and cumulative histograms also for the original configurations (Fig. 4). The regular histograms in the top row do not show any pronounced peaks. The single tall bin at the origin is due to the zero modes which are present in the original configurations. The histograms do not show any strong dependence on the boundary condition. The summation for the cumulative histograms was started at $\text{Im}\lambda = -0.2$ for all boundary con-

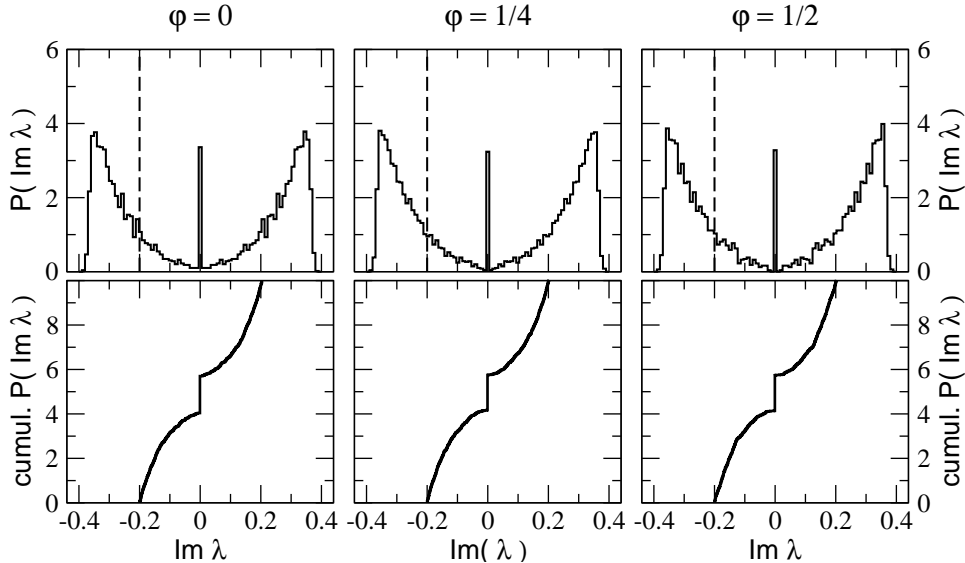


Figure 4: Same as Fig. 3 but now for the original configurations.

ditions. Furthermore, the cumulative histograms are independent of φ and the only feature is the vertical step at $\text{Im}\lambda = 0$ due to the contribution of the zero modes.

3.3 Spectra for random-changed configurations

In Section 2.3 we have discussed the random-changed configurations which we prepared to analyze the effect of an uncorrelated change of the gauge configuration. For $N_{flip} = 1000$ flipped links we find that the action goes up twice as much as when removing the vortices and it is interesting to see what the effects on the spectrum turn out to be.

In Fig. 5 we compare the spectra for a random-changed configuration (lhs. plot) to the spectrum for the original configuration (center plot) and the corresponding vortex-removed configuration (rhs. plot). We used anti-periodic temporal boundary conditions for all three cases. When comparing the spectra of the random-changed and the original configurations, one finds that the former is slightly shifted away from the Ginsparg-Wilson circle and slightly compressed in the vertical direction. Much more important, however, is the fact that the gross features of the two spectra are nearly identical. In particular the number of real eigenvalues, i.e. the number of would be zero modes is invariant, and also the pattern of the relative spacing of the eigenvalues is very similar. This finding does not only hold for a single configuration, but also bulk observables such as the histograms and cumulative histograms for random-changed configurations are very similar to their original counterparts shown in Fig. 4.

We also analyzed the distribution of the topological charge ν in the original

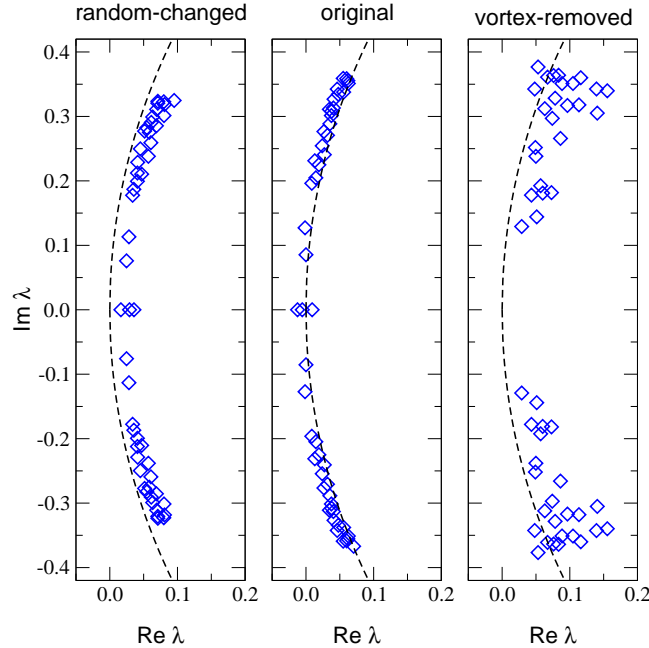


Figure 5: *Dirac eigenvalues λ in the complex plane. We compare the spectrum for the random-changed configuration (lhs. plot), the original configuration (center plot) and the vortex-removed configuration (rhs. plot). The random changes, as well as the procedure of vortex-removal, both started from the same original configuration - the one we also use in the center plot. Anti-periodic temporal boundary conditions were implemented.*

and the random-changed ensemble. The topological charge ν was determined from the index theorem using the difference of the numbers of left-handed and right handed zero modes. The results are displayed in Fig. 6 where we show the distribution of ν for the original configurations in the lhs. plot and for the random-changed configurations in the rhs. plot. Again we observe that the changes due the random alterations of the gauge configuration are minimal. This confirms an earlier finding [28] where it was demonstrated that the topological features of the spectrum of the Wilson Dirac operator are quite stable when adding random noise.

There are certainly many different ways of altering the original configuration for comparison of the effects to a removal of center vortices. Such alternative prescriptions could e.g. be inspired by a particular picture of QCD vacuum excitations. We remark that currently we are exploring such alternative modifications of the gauge field and their effect on the Dirac eigensystem. The random changes we use here are merely intended to demonstrate that a non-correlated change, which increases the action considerably more than removing the vortices, leaves the topological features invariant.

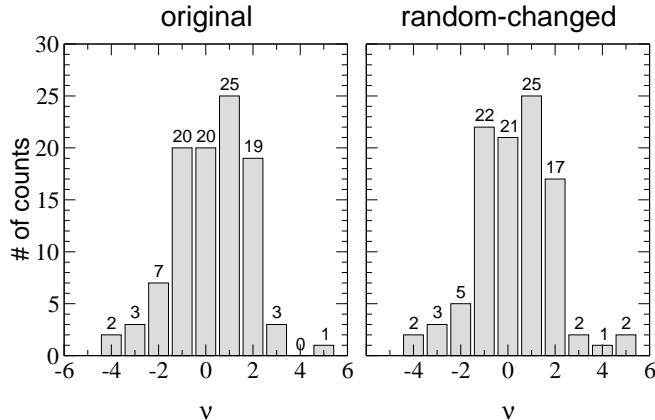


Figure 6: *Distribution of the topological charge ν . We compare data from the original ensemble (lhs. plot) to the random-changed ensemble (rhs. plot).*

4 Results for the Dirac eigenmodes

4.1 Scalar density for zero and near zero modes

After having explored the spectrum for center projected, vortex-removed and random-changed configurations, it is also interesting to study the eigenvectors of the Dirac operator for these ensembles. A suitable observable is the scalar density $\rho(x)$ of an eigenvector \vec{v} . It is defined by summing the color and Dirac indices of \vec{v} at each lattice point x ,

$$\rho(x) = \sum_{c,d} |\vec{v}(x)_{cd}|^2. \quad (8)$$

Since the Dirac operator transforms covariantly under a gauge transformation, the scalar density ρ is gauge invariant.

Since the low-lying Dirac modes do not see large fluctuations of a gauge field, the scalar density of the low-lying Dirac modes can be used as a detector of (smooth) center vortex flux, which does not rely on topological properties of the gauge fields like their topological charge.

In Fig. 7 we show the scalar density over a 2-d slice through the lattice for a zero mode. The lhs. plot is for the original configuration, the rhs. plot after random changes. The slice was chosen such, that it cuts through the maximum of $\rho(x)$. We find a strongly localized lump, which, in an orthodox interpretation, would be the zero mode due to an instanton in the underlying gauge field¹ (see Refs. [29, 30, 31] for an alternative picture.) The lump is essentially unchanged by random changes. Since for the vortex-removed configurations all the zero modes are gone, we cannot produce an equivalent plot for this ensemble.

¹Later we will identify lumps of fractional topological charge with vortex intersection points.

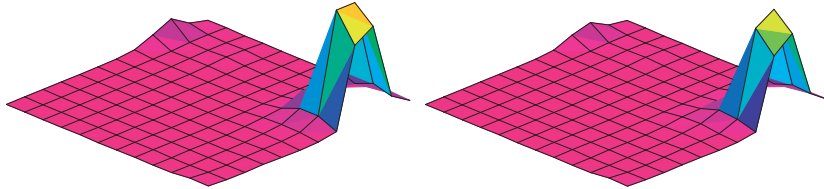


Figure 7: *Plots of the scalar density $\rho(x)$ for the zero-mode of the original configuration (lhs. plot) and the corresponding random-changed configuration (rhs. plot). We show the same 2-d slices for both configurations.*

However, it has long been known that also the “near zero modes”, corresponding to eigenvalues with small but non-vanishing imaginary parts, show lumpy structures². Since also the vortex-removed configurations do have such near zero modes it is possible to compare the scalar density for all four ensembles, original, vortex-removed, random-changed and center projected.

Fig. 8 is such a comparison, with the top left plot showing the original configuration, the top right plot the random-changed configuration, the bottom left plot is for the vortex-removed and the bottom right for the center projected configuration. Again we show a slice through the maximum of ρ . The original and random-changed configurations show pronounced lumps which are located at the same position and have essentially the same shape. When slicing the scalar density for the vortex-removed configuration at the same position we find that the lump is gone completely. In the plot we even stretched the vertical scale by a factor of 10 to make the remaining small wiggles visible at all. Also at other positions on the lattice we do not find localized structures in the near zero modes of vortex-removed configurations. This holds not only for the particular configuration used in Fig. 8, but is a generic feature of the whole ensemble. Thus we must conclude, that removing the vortices also removes the lumpy structures in the eigenmodes. This observation is in agreement with our findings concerning the absence of the chiral condensate: The density of near zero eigenvalues which, according to the Banks-Casher formula, is necessary to build up the chiral condensate, comes from topological objects which perturb each other only slightly. If the chiral condensate is gone for vortex-removed configurations, one expects also a dramatic alteration of the near zero modes. This is exactly what we observe.

Surprisingly, in the center projected configuration the localized lump is also gone. From this one might be tempted to conclude that the topological lump seen in the original lattice configuration is not related to center vortices at all. However, in Section 5 we will provide arguments that, very likely, the topological lumps

²According to the instanton picture these lumps originate from instantons and anti-instantons perturbing each other. This perturbation is, however, only weak, such that locally the near zero mode still resembles the case of the unperturbed instanton.

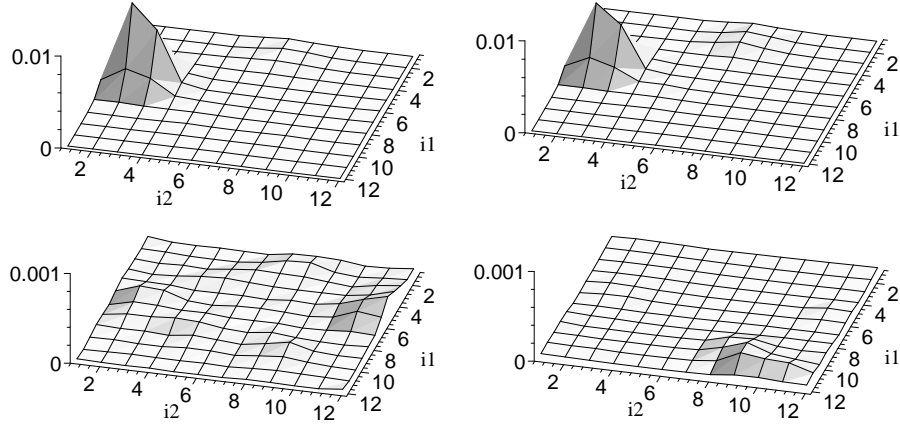


Figure 8: *Plots of the scalar density $\rho(x)$ for a near-zero-mode of the original configuration (top left), as well as the corresponding random-changed (top right), vortex-removed (bottom left) and center projected (bottom right) configurations. We show the same 2-d slice for all four configurations. The vertical axis for the vortex-removed and center projected plot (bottom) is stretched by a factor of 10.*

are not absent in the center projected lattice configuration but are just not seen by the scalar density of the lowest non-zero mode. The reason is that the center projected lattice configurations fluctuate too wildly to be seen by a low energy filter. In Section 5 we will provide arguments supporting this interpretation.

4.2 Local chirality of near zero modes

As addressed above, the low-lying near zero modes are expected to locally resemble true zero modes. In particular, they are expected to be locally chiral. In order to test for local chirality, one can introduce chiral (right- and left-handed) densities $\rho_+(x), \rho_-(x)$, which are obtained by projecting the scalar density $\rho(x)$ to a specific chirality,

$$\rho_{\pm}(x) = \sum_{c,d,d'} \vec{v}(x)_{cd}^* \frac{1}{2} [1 \pm \gamma_5]_{dd'} \vec{v}(x)_{cd'} , \quad (9)$$

where the subscripts denote color and Dirac indices. If the near zero modes are locally chiral, then for a given space-time point x only one of the two densities $\rho_+(x), \rho_-(x)$ is non-zero.

An observable which further analyzes the properties of the near zero modes is the local chirality observable X , introduced in [32, 33] and studied by several groups [34]–[40]. The local chirality variable X is obtained by mapping the ratio

$$r(x) = \frac{\rho_+(x)}{\rho_-(x)} , \quad (10)$$

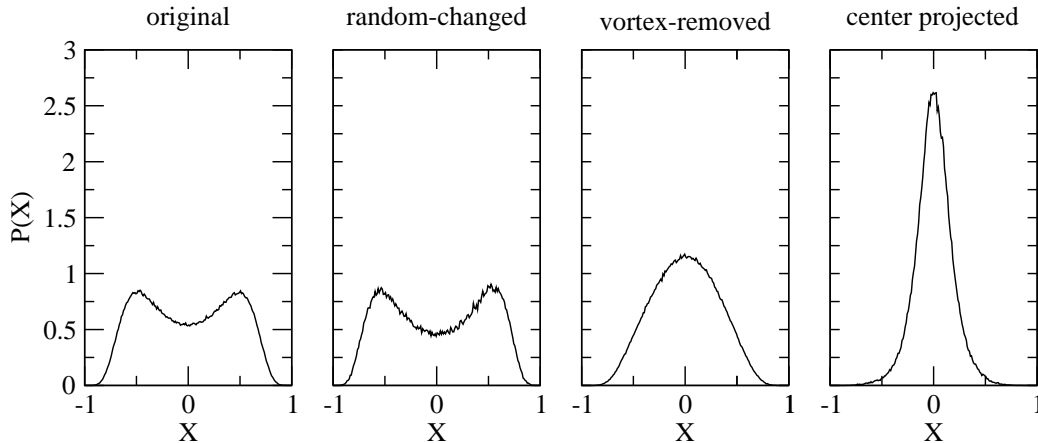


Figure 9: *Distribution of the local chirality variable X . We compare data (from left to right) from the original ensemble to data for the random-changed ensemble, the vortex-removed and center projected configurations.*

which takes values in the interval $[0, \infty)$, to the interval $[-1, 1]$,

$$X(x) = \frac{4}{\pi} \tan^{-1} \left(\sqrt{r(x)} \right) - 1. \quad (11)$$

If the near zero modes are locally chiral, one expects that the distribution of X shows a double peak structure with maxima near ± 1 . If on the other hand the near zero modes are not locally chiral, one expects a single peak near the origin. We determine this distribution using histograms for the values of $X(x)$, where we include all those lattice points x where we find the largest 12.5% of the scalar density. Thus we analyze the local density only for the highest peaks in $\rho(x)$.

The results for the local chirality are shown in Fig. 9. For the original and the random-changed configurations, we find a clear double-peak structure indicating that the near zero modes are locally chiral for these two cases. For the vortex-removed configurations the double-peak structure is gone, indicating that the wiggles in $\rho(x)$ that remain after removing the vortices are not locally chiral structures. This confirms our previous interpretation of these wiggles as structureless fluctuations. As before, we find that the center projected configurations are too singular for an analysis with the low-lying Dirac eigenmodes.

5 Results for smooth center vortices

During the course of our analysis we have found that center projected configurations do not give sensible results when analyzed with the low-lying Dirac eigenmodes. We have argued that center projection yields configurations that are too singular for the eigenmode analysis. This is a consequence of the center projection, which converts the originally fat center vortices (present in the full

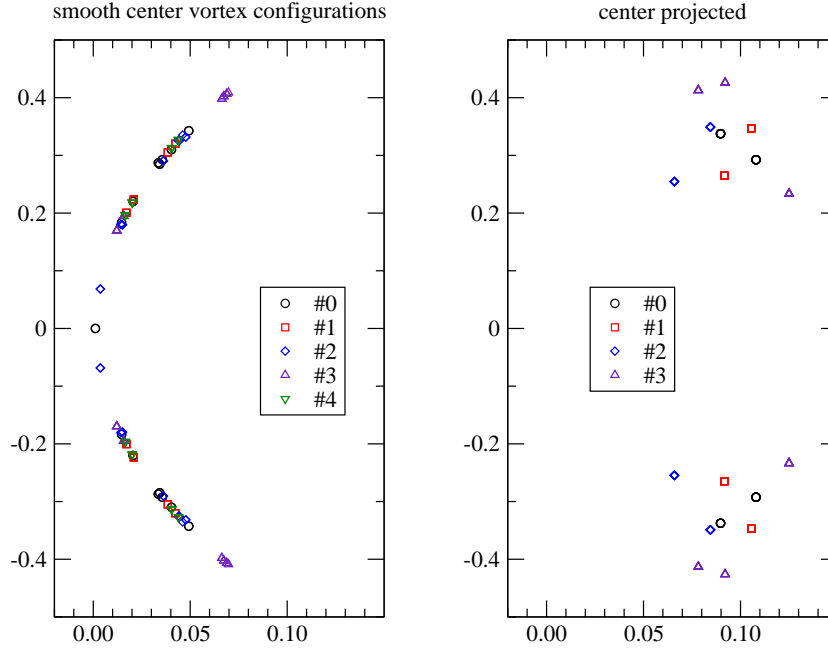


Figure 10: *Dirac spectrum for smooth center vortices (lhs.) and their center projected counter parts (rhs.). Note that the center projection is the same for configurations #0 and #4.*

Yang-Mills ensemble) into “ideal” center vortices, whose transversal extension is one lattice spacing only.

However, in this Section we demonstrate that sufficiently smooth center vortices do indeed produce zero modes and thus can also give rise to chiral symmetry breaking. For this study we use smooth vortex configurations consisting of two pairs of parallel smeared out planar vortex sheets, intersecting perpendicularly in four (smeared out) intersection points, each carrying the topological charge $\pm\frac{1}{2}$ (for more details see Ref. [15]). The vortex sheets are closed by the periodic boundary condition on the 4-torus. The orientation of the vortex sheets, i.e. the direction of the flux is such that the contributions from the intersection points add up to a total topological charge of $\nu = 2$ for configuration #0 and $\nu = 0$ for configurations #1, #2, #3, #4, respectively.

5.1 Spectra of smooth center vortex configurations vs. center projected vortices

Let us begin with analyzing the Dirac spectra for our smooth center vortex configurations. In the lhs. plot of Fig. 10 we show the Dirac spectra for our 5 configurations and compare them to the spectra obtained for the corresponding center projected configurations.

The Dirac spectra of the smeared out center vortex configuration have no

conf.	vortex 1 (k_0, k_3, f)	vortex 2 (k_0, k_3, f)	vortex 3 (k_1, k_2, f)	vortex 4 (k_1, k_2, f)	ν
#0	(10, 14, 0.5)	(4, 14, 0.5)	(4, 4, 0.5)	(12, 14, 0.5)	2
#4	(10, 14, -0.5)	(4, 14, 0.5)	(4, 4, 0.5)	(12, 14, -0.5)	0

Table 1: *Smooth center vortex configurations consisting of 4 planar center vortex sheets which are all parallel to coordinate planes $k_i - k_j$. The table shows the flux f and the coordinates (k_0, k_3) of the two vortices parallel to the $k_1 - k_2$ plane and the coordinates (k_1, k_2) for the two vortices parallel to the $k_0 - k_3$ plane for the configurations #0 and #4. Configuration #4 arises from configuration #0 by changing the orientation of the flux. Furthermore, the total topological charge ν of the configuration is given.*

gap around zero virtuality. In particular, for configuration #0 with non-zero topological charge $\nu = 2$ there is a zero mode, which is two-fold degenerate. After center projection the gap in the Dirac spectra emerges and the zero mode is gone. This is not surprising since in the process of center projection the center vortices lose their orientation and thus their total topological charge, although they still carry the individual local spots of fractional topological charge. But these local contributions will usually add up to zero total charge. This is because orientable closed surfaces in $D = 4$ have zero total self-intersection number, which up to a factor of $\frac{1}{4}$ represents the topological charge of center vortex surfaces [17, 18].

To illustrate the effect of center projection and center vortex removal in more detail we compare in Fig. 11 the Dirac spectrum of the fat center vortex configuration #0 (see Table 1) with topological charge $\nu = 2$ with those of its (b) center projected and (c) center vortex-removed counter parts. For sake of comparison, in Fig. 11(d) we also show the Dirac spectrum of the fat center vortex configuration #4, which has the same vortex surfaces as the configuration #0 (a), however, with different orientations of their fluxes such that $\nu = 0$ (cf. Table 1). Both fat center vortex configurations #0 and #4 have the same center projected and center vortex-removed counter parts and thus the same Dirac spectrum shown in Fig. 11(b) and (c). As is seen, center projection (b) changes the Dirac spectrum as drastically as center vortex removal (c). This is somewhat counter intuitive since the configurations under consideration are plain vortex configurations but, in fact, can be easily understood: The vortex configuration considered in Fig. 11(a), (d) are extremely fat. In the transversal directions they stretch out over the whole lattice. Accordingly, there are only small gradients involved and our lattice Dirac operator works well: all eigenvalues are on the Ginsparg-Wilson circle, see fig 11(a), (d). This property is lost in the center projection, which replaces the originally fat vortices by the ideal (very thin) ones, whose transversal extension is one lattice spacing. Hence the center projected configuration contains large gradients which cannot be properly captured by our Dirac operator. Accordingly

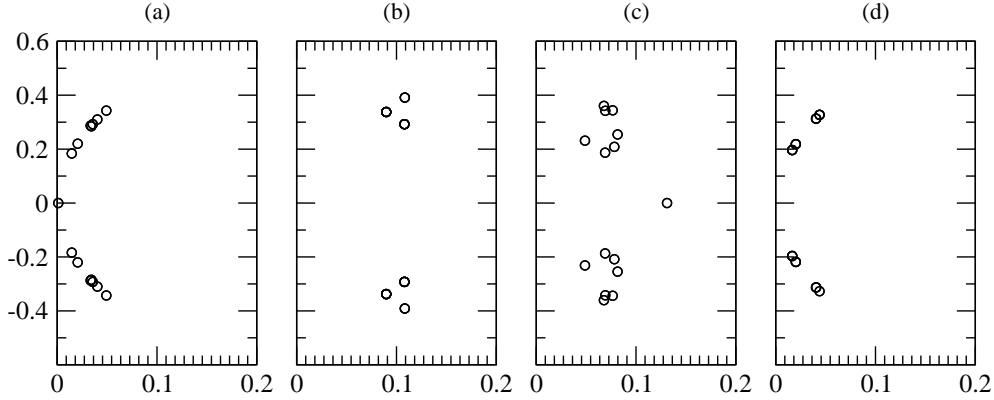


Figure 11: *Dirac spectra of (a) the fat center vortex configuration #0 ($\nu = 2$), its (b) center projected and (c) vortex-removed counter part, and (d) the fat center vortex configuration with $\nu = 0$ obtained from (a) by changing the orientation of the flux.*

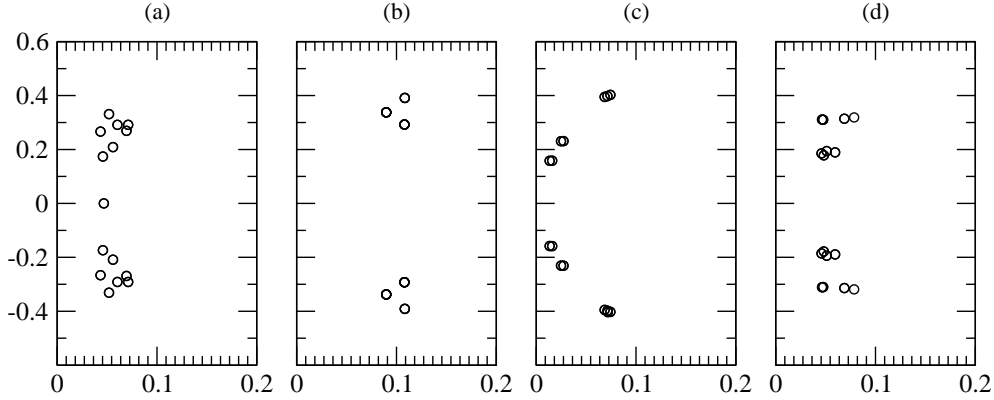


Figure 12: *Dirac spectra for the same fat vortex configuration as in Fig. 11 except that the transversal extension of the vortex flux was shrunk to 2 lattice spacings.*

its eigenvalues are off the Ginsparg-Wilson circle. The method of center vortex “removal” subtracts the ideal center vortices arising in the center projection from the fat vortices. This will give rise to even larger gradients and accordingly the Dirac spectrum Fig. 11(c) will show more “noise.” The method of center vortex removal obviously works the better the thinner the vortices, and becomes perfect for ideal center vortices (having a transversal extension of one lattice spacing)³. The thinner the vortex the less flux is left after vortex removal. To illustrate this we show in Fig. 12 the Dirac spectra for the vortex configurations which result from those considered in Fig. 11 when their transversal vortex extension is shrunk to two lattice spacings. The starting center vortices now have larger gradients

³The method of vortex removal converts an ideal center vortex into the trivial configuration $U_\mu = 1$.

and the Dirac eigenvalues are now shifted off the Ginsparg-Wilson circle. At the same time the Dirac eigenvalues of the vortex-removed configuration Fig. 12 (c) are now basically on the Ginsparg-Wilson circle implying that this configuration contains only little gradients contrary to what we have observed for the very fat vortices (Fig. 11 (c)). For sake of completeness let us also mention that the center projected configurations of the very fat and thin center vortices are the same and so are the corresponding Dirac spectra shown in Fig. 11 (b) and Fig. 12 (b), respectively.

5.2 Eigenvectors

After having demonstrated that for smooth center vortices the spectrum indeed matches the expectation from the index theorem, let us now analyze the corresponding eigenvectors.

Fig. 13 shows the scalar density of the lowest lying non-zero mode of the fat vortex configurations #0 ($\nu = 2$) and #4 ($\nu = 0$) and their center projected image. Both configurations have up to orientation the same vortex flux and thus the same center projected image. The scalar density is shown for a plane which does not coincide with one of the vortex planes. As is seen the scalar density of the lowest non-zero mode detects only one of the two parallel $k_1 - k_2$ flux sheets at $k_0 = 4$ and $k_0 = 1$, and furthermore different sheets for the $\nu = 2$ and $\nu = 0$ configurations. The scalar density of the lowest Dirac mode of the center projected configuration sees both center vortex fluxes and in more pronounced form than the corresponding Dirac mode in the original fat center vortex background. Furthermore, the scalar density is concentrated at the vortex intersection points. These results are in accordance with the findings of Ref. [15] where the concentration of the scalar density of the zero modes near the vortex flux and, in particular, at the intersection points was found. Surprisingly, the scalar density of the center vortex-removed configuration is also localized at the vortex flux and is basically the same as for the center projected configuration. One would have expected that the localized structures arising from the center vortices and their intersections are eliminated by the vortex removal. However, one should keep in mind that vortex removal by the method of Ref. [3], implies subtraction of an ideal center vortex from a fat vortex in the original configuration. If the original vortex is very fat, vortex removal near the vortex core is almost the same as center projection. Only for thin smooth center vortices the vortex removal procedure properly removes the vortex flux.

Fig. 14 shows the scalar density for the same configurations as in Fig. 13, however, for a different 2-d slice which coincides with a vortex plane. In addition, the transversal size of the vortex flux was shrunk to two lattice spacings. Again, the scalar density is localized at the intersection points and is basically the same for original and the center projected configurations while it is suppressed for the vortex-removed configuration, in particular at the intersection points (Note the

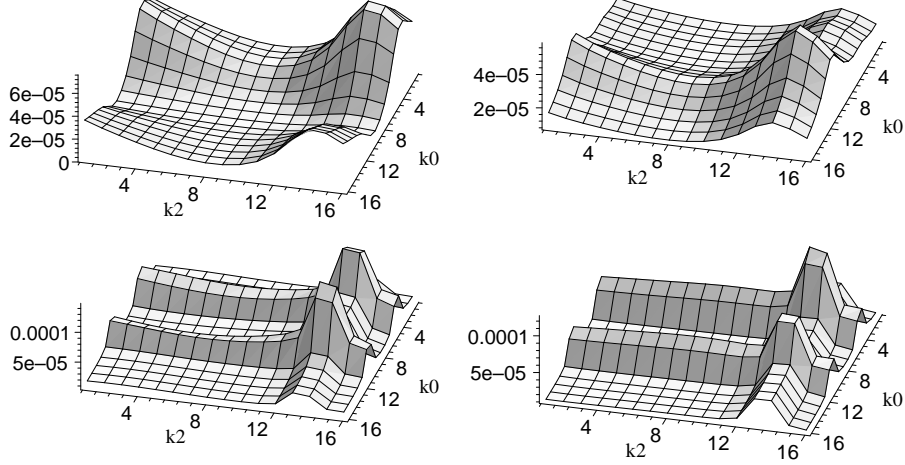


Figure 13: *Plots of the scalar density of the lowest non-zero eigenmodes of configurations #0 (upper left) and #4 (upper right) and of their center projected (lower left) and center vortex-removed counter part (lower right) in the 2-d slice defined by $(k_1, k_3) = (12, 14)$. In this plane the configuration has intersection points at $(k_0, k_2) = (4, 14)$ and $(10, 14)$.*

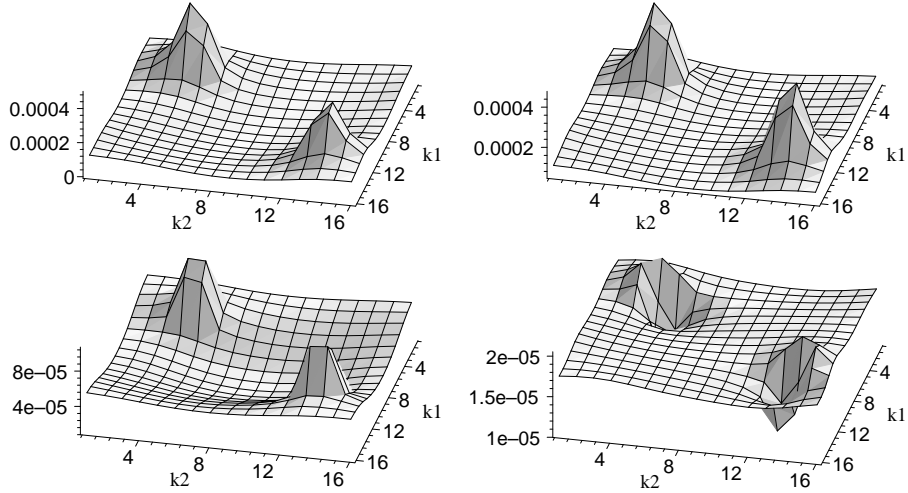


Figure 14: *Plots of the scalar density as in Fig. 13, but in the 2-d slice defined by the second vortex, i.e. $(k_0, k_3) = (4, 14)$, see Table 1. In this plane the configuration has vortex intersection points at $(k_1, k_2) = (4, 4)$ and $(12, 14)$. Furthermore, we show the scalar density of the first non-zero mode for the corresponding vortex-removed configuration (lower right) and of the center projected configuration (lower left).*

different scales!).

Thus for very smooth fat center vortex configurations the center projected vortex surfaces are also smooth and their fluxes and topological spots are very well seen by the scalar density of the near zero modes.

Contrary to the scalar density $\rho(x)$ (8), the chiral densities $\rho_{\pm}(x)$ (9) do feel the orientation of the flux. This can be seen in Fig. 15, where we show the chiral densities of the lowest non-zero Dirac modes of the configurations #0 and #4, which differ only in the orientation of the vortex flux. The chiral densities are shown in a 2-d slice in which these two configurations have two vortex intersection points. For configuration #0 the two vortex intersection points have the same orientation and accordingly give both rise to peaks of the same size in the chiral densities $\rho_{\pm}(x)$. However, the density $\rho_{+}(x)$ is suppressed by a factor of 20 compared to $\rho_{-}(x)$ implying that the considered non-zero Dirac mode is at both vortex intersection points approximately left handed (negative chirality) in agreement with the vortex orientation. For configuration #4 the two intersection points have opposite orientation and we observe a peak in either $\rho_{+}(x)$ or $\rho_{-}(x)$ at the two intersection points. The orientation of the flux is lost in the center projection which hence converts both center vortex configurations #0 and #4 into the same ideal center vortex. Therefore the center projected configurations do not distinguish between $\rho_{+}(x)$ and $\rho_{-}(x)$ and consequently do not reproduce the chiral densities properly. This is indeed seen in Fig. 15 where we compare the chiral densities of the lowest lying non-zero Dirac modes for the fat center vortex configurations #0 and #4, the corresponding center projected and the center vortex-removed configurations.

6 Summary and Conclusions

Using the chirally improved Dirac operator constructed in [19, 20], we have studied the influence of center vortices on various properties of the Dirac spectrum. We have shown that removal of center vortices eliminates the zero modes and near zero modes of the Dirac operator. Via the Banks-Casher relation this implies the restoration of chiral symmetry. We have demonstrated that the spectrum for vortex-removed configurations strongly resembles the free Dirac spectrum. For the Dirac eigenmodes we found that removing the center vortices destroys local chirality of the low lying modes. Comparison with configurations, subject to incoherent random changes, shows that removing the center vortices specifically targets the topological properties, while random changes leave them intact.

Somewhat surprisingly we find that also center projection eliminates the topological charge and gives rise to a gap near zero virtuality. However, this result does not mean that center vortices are not responsible for the topological properties of the gauge fields and for the spontaneous breaking of chiral symmetry but can be traced back to the fact that center projection removes the orientation of

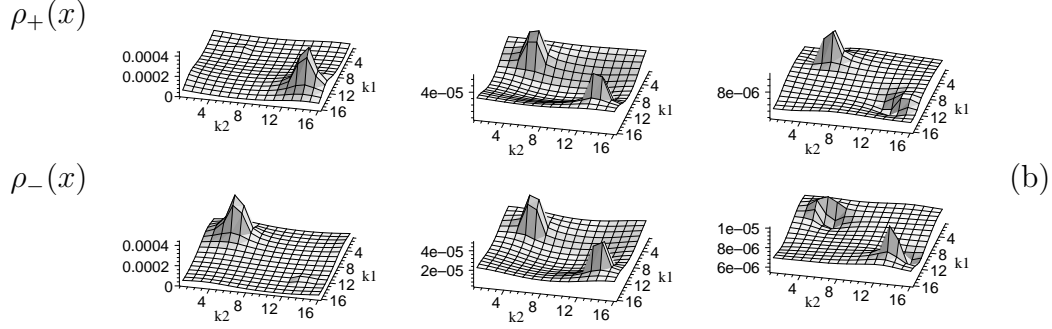
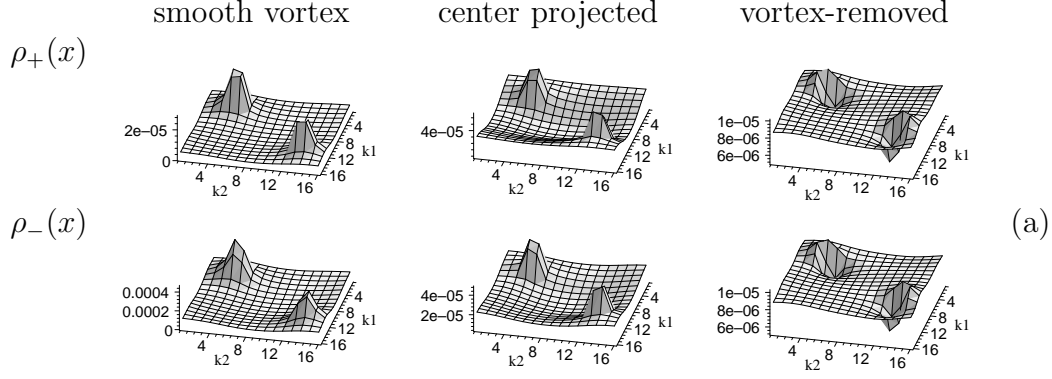


Figure 15: (a) Plots of the chiral densities $\rho_+(x)$ (upper row) and $\rho_-(x)$ (lower row) of the lowest non-zero Dirac mode for the configuration #0 and its center projected and vortex-removed counter parts through the 2-d slice defined by the plane $(k_0, k_3) = (4, 14)$, in which this configuration has two vortex intersection points. Note that in the upper left plot the density $\rho_+(x)$ was stretched by a factor of 20. (b) The same as in (a) for configuration #4.

the vortices. Center projection keeps track, however, of the module of the flux of the vortices. This was demonstrated by measuring the scalar density of the lowest-lying non-zero modes, which is insensitive to the direction of the flux. The center projected configurations show the same localization of the scalar density near the center vortices (and their intersection points) as the full configurations when the latter are rather smooth. While the center projected configurations reproduce the localization of the scalar density near the vortices, they do not reproduce the localization of the chiral densities, as the latter depend on the orientation of the flux. The orientation of the flux of the center vortices is irrelevant for their confining properties but crucial for their topological and chiral properties. Therefore we arrive at the conclusion that the familiar method of center projection is not suited to study the chiral and topological properties of center vortices for lattice ensembles. To capture the topological properties one has, at least, to embed the center configurations into the Cartan subgroup to preserve the orientation of the center surfaces.

Acknowledgments:

We thank Manfred Faber, Meinulf Göckeler, Christian Lang, Rainer Pullirsch and Pierre van Baal for discussions. The calculations were done on the Hitachi SR8000 at the Leibniz Rechenzentrum in Munich and we thank the LRZ staff for training and support. This work was supported by the DFG Forschergruppe “Lattice-Hadron-Phenomenology” and by DFG - Re856/5-1.

References

- [1] L. Del Debbio, M. Faber, J. Greensite and S. Olejnik, Phys. Rev. **D55**, 2298 (1997)
- [2] K. Langfeld, H. Reinhardt and O. Tennert, Phys. Lett. B **419**, 317 (1998)
- [3] P. de Forcrand and M. D’Elia, Phys. Rev. Lett. **82**, 4582 (1999)
- [4] K. Langfeld, H. Reinhardt and J. Gattnar, Nucl. Phys. B **621**, 131 (2002)
- [5] J. Gattnar, K. Langfeld and H. Reinhardt, Phys. Rev. Lett. **93**, 061601 (2004)
- [6] J. Greensite, S. Olejnik and D. Zwanziger, arXiv:hep-lat/0407032
- [7] K. Langfeld, O. Tennert, M. Engelhardt and H. Reinhardt, Phys. Lett. B **452**, 301 (1999)

- [8] M. Engelhardt, K. Langfeld, H. Reinhardt and O. Tennert, Phys. Rev. D **61**, 054504 (2000)
- [9] K. Langfeld, Phys. Rev. D **67**, 111501 (2003)
- [10] J. Gattnar, K. Langfeld, A. Schafke and H. Reinhardt, Phys. Lett. B **489**, 251 (2000)
- [11] M. Engelhardt and H. Reinhardt, Nucl. Phys. B **585**, 591 (2000)
- [12] M. Engelhardt, M. Quandt and H. Reinhardt, Nucl. Phys. B **685**, 227 (2004)
- [13] T. G. Kovacs and E. T. Tomboulis, Phys. Rev. Lett. **85**, 704 (2000)
- [14] J. D. Lange, M. Engelhardt and H. Reinhardt, Phys. Rev. D **68**, 025001 (2003)
- [15] H. Reinhardt, O. Schroeder, T. Tok and V. C. Zhukovsky, Phys. Rev. D **66**, 085004 (2002)
- [16] L. Del Debbio, M. Faber, J. Giedt, J. Greensite and S. Olejnik, Phys. Rev. D **58**, 094501 (1998)
- [17] M. Engelhardt and H. Reinhardt, Nucl. Phys. B **567**, 249 (2000)
- [18] H. Reinhardt, Nucl. Phys. B **628**, 133 (2002)
- [19] C. Gattringer, Phys. Rev. D **63**, 114501 (2001)
- [20] C. Gattringer, I. Hip and C. B. Lang, Nucl. Phys. B **597**, 451 (2001)
- [21] C. Gattringer, M. Göckeler, C. B. Lang, P. E. L. Rakow and A. Schäfer, Phys. Lett. B **522**, 194 (2001)
- [22] D.C. Sorensen, SIAM J. Matrix, Anal. Appl. **13**, 357 (1992)
- [23] C. Gattringer, Phys. Rev. D **67**, 034507 (2003)
- [24] C. Gattringer and S. Schaefer, Nucl. Phys. B **654**, 30 (2003)
- [25] C. Gattringer and R. Pullirsch, Phys. Rev. D **69**, 094510 (2004)
- [26] C. Gattringer and S. Solbrig, arXiv:hep-lat/0410040
- [27] T. Banks and A. Casher, Nucl. Phys. B **169**, 103 (1980)
- [28] C. Gattringer and I. Hip, Nucl. Phys. B **536**, 363 (1998)
- [29] I. Horvath *et al.*, Phys. Rev. D **68**, 114505 (2003)

- [30] I. Horvath, S. J. Dong, T. Draper, F. X. Lee, K. F. Liu, H. B. Thacker and J. B. Zhang, Phys. Rev. D **67**, 011501 (2003)
- [31] C. Aubin *et al.* [MILC Collaboration], arXiv:hep-lat/0410024
- [32] I. Horvath, N. Isgur, J. McCune and H. B. Thacker, Phys. Rev. D **65**, 014502 (2002)
- [33] I. Horvath *et al.*, Phys. Rev. D **66**, 034501 (2002)
- [34] T. DeGrand and A. Hasenfratz, Phys. Rev. D **65**, 014503 (2002)
- [35] T. Blum *et al.*, Phys. Rev. D **65**, 014504 (2002)
- [36] R. G. Edwards and U. M. Heller, Phys. Rev. D **65**, 014505 (2002)
- [37] I. Hip, T. Lippert, H. Neff, K. Schilling and W. Schroers, Phys. Rev. D **65**, 014506 (2002)
- [38] C. Gattringer, M. Göckeler, P. E. L. Rakow, S. Schaefer and A. Schäfer, Nucl. Phys. B **617**, 101 (2001)
- [39] C. Gattringer, M. Göckeler, P. E. L. Rakow, S. Schaefer and A. Schäfer, Nucl. Phys. B **618**, 205 (2001)
- [40] P. Hasenfratz, S. Hauswirth, K. Holland, T. Jörg and F. Niedermayer, Nucl. Phys. Proc. Suppl. **106**, 751 (2002)